INTERNATIONAL JOURNAL FOR NUMERICAL AND ANALYTICAL METHODS IN GEOMECHANICS
Int. J. Numer. Anal. Meth. Geomech. 2012; **36**:85–99
Published online 7 December 2010 in Wiley Online Library (wileyonlinelibrary.com). DOI: 10.1002/nag.994

Heat extraction from aquifer geothermal systems

Hund-Der Yeh[1], Shaw-Yang Yang[2,*,†] and Kuang-Yi Li[1]

[1]*Institute of Environmental Engineering, National Chiao Tung University, Hsinchu 300, Taiwan*
[2]*Department of Civil Engineering, Vanung University, Chungli 320, Taiwan*

SUMMARY

This study aims to model temperature distributions in an aquifer thermal extraction (ATE) system that contains a single extraction well in a thin confined aquifer. The aquifer is bounded by hot dry rocks with different thermomechanical properties and thicknesses. Based on the heat convection–conduction equation, a mathematical model is developed to describe the spatial and temporal temperature distributions of the ATE systems. The mechanisms of heat transfer in the model involve horizontal convection and thermal conduction in the aquifer, and vertical thermal conduction in both rocks. A semi-analytical solution in dimensionless form is developed using the Laplace transform technique and its corresponding time-domain result is computed by the modified Crump method. In addition, the steady-state solution is obtained by applying the final value theorem. The simulation results from the semi-analytical solution indicate that the aquifer temperature distributions are affected by aquifer thickness, the thermomechanical properties of the aquifer and rocks, geothermal gradient, outer boundary temperatures of the rocks, extraction rate, and operating time. The present solution can be used as a preliminary tool for assessing heat extraction efficiency in ATE systems. Copyright © 2010 John Wiley & Sons, Ltd.

Received 21 March 2010; Revised 22 June 2010; Accepted 11 October 2010

KEY WORDS: geothermal extraction; semi-analytical solution; heat transfer; aquifer thermal extraction (ATE)

1. INTRODUCTION

Heat extraction from geothermal energy resources through aquifer thermal extraction (ATE) systems is an alternative to obtain thermal energy. Therefore, the extraction efficiency of an ATE system must be estimated prior to operation.

Sauty *et al.* [1] presented a theoretical study of the thermal behavior of hot water storage in an aquifer. A finite difference model was used to predict the well temperature during various production periods. In addition, Sauty *et al.* [2] performed field experiments on hot water storage and compared the experimental results with theoretical predictions given by Sauty *et al.* [1]. Carotenuto *et al.* [3] conducted some experiments on a geothermal exchanger system for heat extraction from an aquifer without fluid withdrawal. They estimated the heat flow between cold and warm fluids in the aquifer using the finite element method. Tenma *et al.* [4] presented a simulation model to design a thermal storage system in low-temperature geothermal resources and evaluated the sensitivity of the results to parameters, such as well distance, well depth, and flow rate. They used the FEHM (Finite Element Heat and Mass transfer) code developed by Zyvoloski *et al.* [5] to simulate heat and mass transfers in porous media. Furthermore, Tenma *et al.* [6] conducted field tests in a hot dry rock (HDR) system in Hijiori, Japan, to optimize heat extraction effectiveness in a two-layered reservoir. They found that the best option for heat extraction is to increase the flow rate into the deep reservoirs.

*Correspondence to: Shaw-Yang Yang, Department of Civil Engineering, Vanung University, Chungli 320, Taiwan.
†E-mail: shaoyang@vnu.edu.tw

Yang and Yeh [7] presented a mathematical model to simulate thermal energy transfer from the injection of hot water into a confined aquifer with different geological properties in the underlying and overlying rocks. Their model involves the transfer mechanisms of horizontal convection in the radial aquifer and vertical conduction in the confining rocks. Yang and Yeh [8] also developed an analytical model describing heat energy extraction from an HDR in a multi-well system. They found that heat extraction effectiveness is affected by well spacing, well radius, reservoir thickness, and pumping rate.

Ghassemi *et al.* [9] utilized an integral equation formulation with a Green's function to simulate the heat extraction by circulating water in a fracture embedded in a geothermal reservoir. Ghassemi and Kumar [10] examined the changes in fracture aperture and fluid pressure caused by the individual and combined influences of thermal stress and chemical processes resulting from heat extraction from subsurface rocks. Furthermore, Ghassemi *et al.* [11] presented a porothermoelastic model to explore hydrothermomechanics in response to cold water injection in an enhanced (or engineered) geothermal system. They investigated the changes in fracture aperture caused by cooling and fluid leak-off into adjacent rocks. Yin *et al.* [12] developed a fully coupled, thermal half-space model based on a finite element method and a displace discontinuity method to analyze stress, pressure, temperature, and volume change in thermal reservoirs.

The objective of this study is to develop a mathematical model describing the temperature distribution in an ATE system after extracting hot water from a geothermal confined aquifer. The model assumes that an extraction well fully penetrates the confined aquifer, which is underlain and overlain by finite-thickness HDRs with different thermomechanical properties and geothermal gradients in the vertical direction. The outer boundaries of the overlying and underlying rocks are represented by the Robin boundary condition. Heat energy is partially captured from the aquifer and transferred from adjacent rocks to the water of the aquifer. The solution of the model in dimensionless form is developed by the Laplace transform technique and its corresponding result domain is computed by the modified Crump method [13, 14]. The present solution can be used to simulate the spatial and temporal temperature distribution in ATE systems and assess the influences of geological parameters as well as thermal properties on temperature distribution.

2. ANALYTICAL STUDY

2.1. Conceptual model

Figure 1 shows a schematic representation of the ATE system composed of a thin confined aquifer underlain and overlain by two different HDRs. The aquifer and rocks extend infinitely in the horizontal direction. The rocks are impermeable and the geological parameters as well as the thermal properties of the aquifer and rocks are temperature invariant. In addition, the rocks are considered to have linear geothermal gradients in the vertical depth and the initial temperature in the aquifer is uniformly distributed because the aquifer is thin. Heat transfer occurs due to horizontal convection and thermal conduction in the aquifer. In addition, only vertical thermal conduction occurs between the rock and the aquifer. A finite-radius extraction well is installed and screened throughout the confined aquifer. Water is pumped through the extraction well with a constant flow rate Q from the aquifer over the operating time. The water temperature is assumed uniform throughout the entire wellbore. In addition, the geomechanical effects produced by the well discharge are assumed negligible.

The heat convection–conduction equation describing aquifer temperature distribution in the ATE system can be written as [15, p. 25]

$$b_m\left[(\rho c)_m\left(\frac{\partial T_m(r,t)}{\partial t}+u\frac{\partial T_m(r,t)}{\partial r}\right)-K_m\left(\frac{\partial^2 T_m(r,t)}{\partial r^2}+\frac{1}{r}\frac{\partial T_m(r,t)}{\partial r}\right)\right]$$
$$=-K_1\left.\frac{\partial T_1(r,z,t)}{\partial z}\right|_{z=0}+K_2\left.\frac{\partial T_2(r,z,t)}{\partial z}\right|_{z=b_m} \quad (1)$$

DOI: 10.1002/nag

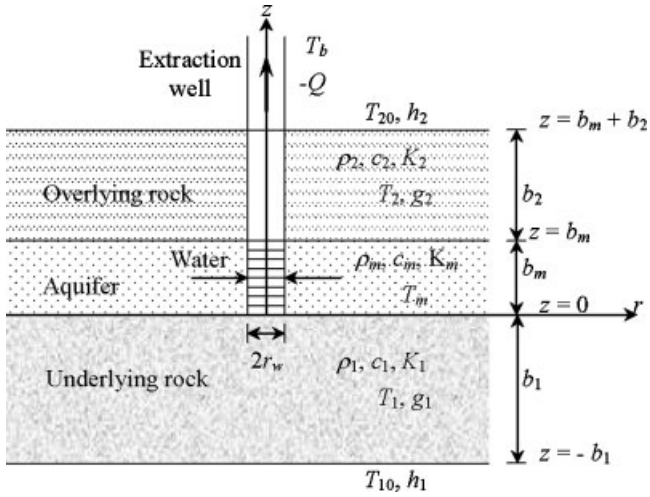

Figure 1. Schematic representation of an aquifer thermal extraction system.

where the subscripts m, 1, and 2 denote the aquifer, underlying rock, and overlying rock, respectively; T is the temperature; b is the thickness; K is the thermal conductivity; ρc is the thermal capacity; r is the radial distance from the center of the extraction well; z is the vertical distance from the bottom of the aquifer; and t is the operating time. The volumetric flux per unit pore area within the confined aquifer, i.e. flow velocity u, is equal to $-Q/(2\pi r n b_m)$, where n is the aquifer porosity and the negative sign indicates that the flow is in the opposite direction of the coordinate.

The initial temperature is expressed as

$$T_m(r,0)=T_{m0} \tag{2}$$

where T_{m0} is a constant temperature.

The continuity of the total heat flux between the extraction wellbore and the aquifer requires

$$-K_m\frac{\partial T_m(r_w,t)}{\partial r}=(\rho c)_m u(r=r_w)[T_m(r_w,t)-T_{m0}] \tag{3}$$

The aquifer temperature maintains a constant value at infinity, i.e. the initial temperature. Such a boundary condition is expressed as

$$T_m(\infty,t)=T_{m0} \tag{4}$$

The heat conduction equation describing the temperature distribution in the underlying rock can be written as [15, p. 8]

$$\frac{\partial^2 T_1(r,z,t)}{\partial z^2}=\frac{(\rho c)_1}{K_1}\frac{\partial T_1(r,z,t)}{\partial t} \tag{5}$$

Considering the presence of a geothermal gradient, the initial temperature distribution in the underlying rock can be expressed as

$$T_1(r,z,0)=T_{m0}-g_1 z, \quad -b_1<z<0 \tag{6}$$

where g_1 represents the geothermal gradient in the underlying rock.

Consider that there is a perfect thermal contact at the interface between the underlying rock and the aquifer such that the heat transfer is very large; therefore, the continuity of the temperature at the interface can be expressed as

$$T_1(r,0,t)=T_m(r,t) \tag{7}$$

DOI: 10.1002/nag

At the lower boundary in the underlying rock, a Robin-type condition employed to specify the unknown total heat flux across the boundary is [15, p. 17]

$$-K_1\frac{\partial T_1(r,-b_1,t)}{\partial z}=-h_1[T_1(r,-b_1,t)-T_{10}] \tag{8}$$

where h_1 is the convective heat transfer coefficient of the underlying rock. The convective heat flux, the term on the right-hand side of Equation (8), is proportional to the difference between the outer boundary temperature and the surface temperature of the underlying rock, T_{10}, which can be expressed as $T_{10}=T_{m0}+g_1b_1$.

Similarly, the heat conduction equation describing the temperature distribution in the overlying rock can be written as [15, p. 8]

$$\frac{\partial^2 T_2(r,z,t)}{\partial z^2}=\frac{(\rho c)_2}{K_2}\frac{\partial T_2(r,z,t)}{\partial t} \tag{9}$$

which is subject to the following initial and boundary conditions:

$$T_2(r,z,0)=T_{m0}-g_2z,\quad b_m<z<b_m+b_2 \tag{10}$$

$$T_2(r,b_m,t)=T_m(r,t)\text{ at the lower boundary} \tag{11}$$

and

$$-K_2\frac{\partial T_2(r,b_m+b_2,t)}{\partial z}=h_2[T_2(r,b_m+b_2,t)-T_{20}]\text{ at the upper boundary} \tag{12}$$

where h_2 is the convective heat transfer coefficient of the overlying rock and T_{20}, the atmospheric or surface temperature of the overlying rock, is expressed as $T_{20}=T_{m0}-g_2(b_m+b_2)$ with the variable g_2 representing the geothermal gradient in the overlying rock.

2.2. Laplace-domain solutions

The Laplace-domain solutions for the temperature distributions of various problems are mentioned in related handbooks [15–17]. Here, using the normalized parameters listed in Table I, Equations (1)–(12) can be expressed in dimensionless forms. A description of the detailed developments of the Laplace-domain solutions for the aquifer, underlying rock, and overlying rock is given in Appendix A. The final dimensionless solution of the aquifer temperature distribution in the Laplace domain is

$$\bar{T}_{mD}(R,p)=-\frac{1}{p}\left(\frac{R_w}{R}\right)^v\left[\frac{2vK_v(\sqrt{A(p)}R)}{2vK_v(\sqrt{A(p)}R_w)+(\sqrt{A(p)}R_w)K_{v-1}(\sqrt{A(p)}R_w)}\right]\left[\frac{B(p)}{A(p)}\right]-\frac{B(p)}{pA(p)} \tag{13}$$

with

$$A(p)=p+K_{1D}q_1x_1+K_{2D}q_2x_2 \tag{14}$$

and

$$B(p)=K_{1D}q_1y_1\lfloor 4T_{1g}(1+\beta_1B_1)-\beta_1T_{10D}\rfloor-K_{2D}q_2y_2\lfloor 4T_{2g}(1+\beta_2+\beta_2B_2)+\beta_2T_{20D}\rfloor -K_{1D}T_{1g}+K_{2D}T_{2g}+4K_{2D}T_{2g}q_2x_2 \tag{15}$$

DOI: 10.1002/nag

Table I. Normalized parameters used in this study.

$T_{mD}(R,\tau)=\frac{T_m(r,t)-T_{m0}}{T_b-T_{m0}}$,	$T_{1D}(R,Z_1,\tau)=\frac{T_1(r,z,t)-T_{m0}}{T_b-T_{m0}}$,	$T_{2D}(R,Z_2,\tau)=\frac{T_2(r,z,t)-T_{m0}}{T_b-T_{m0}}$		
$T_{10D}=\frac{T_{10}-T_{m0}}{T_b-T_{m0}}$,	$T_{20D}=\frac{T_{20}-T_{m0}}{T_b-T_{m0}}$,	$T_{1g}=\frac{g_1 b_m}{4(T_b-T_{m0})}$,	$T_{2g}=\frac{g_2 b_m}{4(T_b-T_{m0})}$	
$R=\frac{2r}{b_m}$,	$R_w=\frac{2r_w}{b_m}$,	$Z_1=-\frac{4z}{b_m}$,	$Z_2=\frac{4(z-b_m)}{b_m}$,	$\tau=\frac{4\alpha_m t}{b_m^2}$, $v=-\frac{Q(\rho c)_m}{4\pi n b_m K_m}$
$\alpha_m=\frac{K_m}{(\rho c)_m}$,	$\alpha_1=\frac{K_1}{(\rho c)_1}$,	$\alpha_2=\frac{K_2}{(\rho c)_2}$,	$\alpha_{1D}=\frac{4\alpha_1}{\alpha_m}$,	$\alpha_{2D}=\frac{4\alpha_2}{\alpha_m}$, $\beta_1=\frac{h_1 b_m}{K_1}$, $\beta_2=\frac{h_2 b_m}{K_2}$
$B_1=\frac{b_1}{b_m}$,	$B_2=\frac{b_2}{b_m}$,	$K_{1D}=\frac{K_1}{K_m}$,	$K_{2D}=\frac{K_2}{K_m}$	

where p is the Laplace variable [18]; $K_v(\cdot)$ is the modified Bessel function of the second kind with order v; $q_i^2=p/\alpha_{iD}$; and $x_i=[4q_i\sinh(4q_iB_i)+\beta_i\cosh(4q_iB_i)]y_i$ with $y_i=1/[4q_i\cosh(4q_iB_i)+\beta_i\sinh(4q_iB_i)]$, where $i=1,2$. In addition, the Laplace-domain solutions of dimensionless temperature distribution in the underlying and overlying rocks are, respectively,

$$\bar{T}_{1D}(R,Z_1,p)=\bar{T}_{mD}(R,p)y_1\{4q_1\cosh[q_1(4B_1-Z_1)]+\beta_1\sinh[q_1(4B_1-Z_1)]\}$$
$$-\frac{\sinh(q_1Z_1)}{p}y_1[4T_{1g}(1+\beta_1B_1)-\beta_1T_{10D}]+\frac{T_{1g}}{p}Z_1 \tag{16}$$

and

$$\bar{T}_{2D}(R,Z_2,p)=\left(\bar{T}_{mD}(R,p)+\frac{4T_{2g}}{p}\right)y_2\{4q_2\cosh[q_2(4B_2-Z_2)]+\beta_2\sinh[q_2(4B_2-Z_2)]\}$$
$$+\frac{\sinh(q_2Z_2)}{p}y_2[4T_{2g}(1+\beta_2+\beta_2B_2)+\beta_2T_{20D}]-\frac{T_{2g}}{p}(Z_2+4) \tag{17}$$

Note that Equations (16) and (17) include the aquifer temperature distribution, $\bar{T}_{mD}(R,p)$, given by Equation (13).

2.3. Steady-state solution

The steady-state solution of dimensionless aquifer temperature distribution can be obtained from Equation (13) by applying the final value theorem [19]. The detailed development of the steady-state solution of dimensionless aquifer temperature is shown in Appendix B and the result is

$$T_{mD}(R,\infty)=-\left(\frac{R_w}{R}\right)^v\left[\frac{2vK_v(\sqrt{A(0)}R)}{2vK_v(\sqrt{A(0)}R_w)+(\sqrt{A(0)}R_w)K_{v-1}(\sqrt{A(0)}R_w)}\right]\left[\frac{B(0)}{A(0)}\right]-\frac{B(0)}{A(0)} \tag{18}$$

with

$$A(0)=K_{1D}\beta_1x+K_{2D}\beta_2y \tag{19}$$

and

$$B(0)=K_{1D}x\lfloor 4T_{1g}(1+\beta_1B_1)-\beta_1T_{10D}\rfloor-K_{2D}y\lfloor 4T_{2g}(1+\beta_2+\beta_2B_2)+\beta_2T_{20D}\rfloor$$
$$-K_{1D}T_{1g}+K_{2D}T_{2g}+4K_{2D}T_{2g}\beta_2y \tag{20}$$

where $x=1/4(1+\beta_1B_1)$ and $y=1/4(1+\beta_2B_2)$.

Similarly, the steady-state solutions for the temperature distributions in the underlying and overlying rocks can be derived from Equations (16) and (17), respectively, as

$$T_{1D}(R,Z_1,\infty)=\left[1-\frac{\beta_1Z_1}{4(1+\beta_1B_1)}\right]T_{mD}(R,\infty)+\frac{\beta_1Z_1}{4(1+\beta_1B_1)}T_{10D} \tag{21}$$

DOI: 10.1002/nag

and

$$T_{2D}(R, Z_2, \infty) = \left[1 - \frac{\beta_2 Z_2}{4\left(1+\beta_2 B_2\right)}\right] T_{mD}(R, \infty) + \frac{\beta_2 Z_2}{4(1+\beta_2 B_2)} T_{20D} \tag{22}$$

3. NUMERICAL INVERSION OF THE LAPLACE-DOMAIN SOLUTIONS

Equations (13), (16), and (17) comprise hyperbolic functions (e.g. sinh(·) and cosh(·)) and Bessel functions $K_v(\cdot)$; thus their time-domain solutions may not be tractable. The routine DINLAP of IMSL [20], developed based on a numerical algorithm originally proposed by Crump [13] and later modified by de Hoog *et al.* [14], is used to obtain the results domain. This routine has been successfully applied to solve some groundwater problems [21, 22]. This algorithm approximates the Laplace inversion by expressing the inverted function in terms of a Fourier series and accelerates the calculation using the Shanks method [23]. Equations (13), (16), and (17) are computed numerically with accuracy to the fourth decimal.

The order v of Bessel function $K_v(\zeta)$ in Equations (13), (16), and (17) is a dimensionless nonintegral convective parameter, denoted as $-Q(\rho c)_m/(4\pi n b_m K_m)$. Using an ascending series for $I_v(\zeta)$, the term $K_v(\zeta)$ given by Abramowitz and Stegun [24, p. 375] can be rewritten as

$$K_v(\zeta) = \frac{\pi}{2} \frac{I_{-v}(\zeta) - I_v(\zeta)}{\sin(v\pi)} \tag{23}$$

with

$$I_v(\zeta) = \left(\frac{\zeta}{2}\right)^v \sum_{k=0}^{\infty} \frac{\left(\frac{1}{4}\zeta^2\right)^k}{k!\Gamma(v+k+1)} \tag{24}$$

where $\Gamma(\cdot)$ is the Gamma function. As $|\zeta|$ is large, $K_v(\zeta)$ tends to be infinity. Using asymptotic expansion of a large argument, $K_v(\zeta)$ can be approximated as [24, p. 378]

$$K_v(\zeta) = \sqrt{\frac{\pi}{2\zeta}} \mathrm{e}^{-\zeta} \left\{1 + \frac{\lambda-1}{8\zeta} + \frac{(\lambda-1)(\lambda-9)}{2!(8\zeta)^2} + \frac{(\lambda-1)(\lambda-9)(\lambda-25)}{3!(8\zeta)^3} + \cdots\right\}, \left(|\arg\zeta| < \frac{3}{2}\pi\right) \tag{25}$$

where $\lambda = 4v^2$. The calculation of Equation (25) for summing the infinite terms is laborious. The Shanks method is again adopted to accelerate the calculation in this equation. This method has been successfully used to study groundwater area [25, 26].

4. RESULTS AND DISCUSSION

Consider that the ATE system has a well radius $r_w = 0.05\,\mathrm{m}$ with the extraction rate $Q = 1 \times 10^{-4}\,\mathrm{m}^3/\mathrm{s}$. The aquifer thickness b_m is 10 m while the thicknesses of the upper rock b_1 and the lower rock b_2 are 50 and 40 m, respectively. The confined aquifer has an initial temperature of 70°C and the hot water in the aquifer is continuously pumped out from the extraction well. The outer boundary temperature of the underlying rock varies with the constant gradient while that of the overlying rock has a fixed temperature of 23°C. We investigate the influences of aquifer thickness, geothermal gradients, and the outer boundary temperature of the rocks on heat extraction efficiency. The thermomechanical properties of the aquifer and rocks listed in Table II are used in the following case studies. The extracted temperature, T_w, is defined as the temperature located at 0.05 m from the rim of the extraction well.

The contour of temperature distribution in the ATE system is shown in Figure 2 for $Q = 1 \times 10^{-4}\,\mathrm{m}^3/\mathrm{s}$ and $1 \times 10^{-3}\,\mathrm{m}^3/\mathrm{s}$ at the operating time $t = 10^4$ days. The thermal front is defined as the distance from the center line of a well to the location at a temperature of 51.0°C. The

DOI: 10.1002/nag

Table II. Parameter values of the aquifer and rocks.

Parameter name	Symbol	Value
Thickness of the aquifer	b_m	10 m
Thickness of the rocks	b_1, b_2	50, 40 m
Density of the aquifer	ρ_m	1047 kg/m^3
Density of the rocks	ρ_1, ρ_2	2600, 2650 kg/m^3
Specific heat of the aquifer	c_m	2713 J/kg·K
Specific heat of the rocks	c_1, c_2	800, 1046 J/kg·K
Thermal conductivity of the aquifer	K_m	2.4 W/m·K
Thermal conductivity of the rocks	K_1, K_2	1.5, 2.59 W/m·K
Convective heat transfer coefficient of the rocks	h_1, h_2	0.6, 1.0 W/m^2·K
Geothermal gradient of the rocks	g_1, g_2	0.03, 0.06°C/m
Porosity of the aquifer	n	0.3

thermal front in the aquifer is located at radial distance$r$ = 12 m for $Q=1\times10^{-4}\,\mathrm{m}^3/\mathrm{s}$ shown in Figure 2(a) and at $r=45\,\mathrm{m}$ for $Q=1\times10^{-3}\,\mathrm{m}^3/\mathrm{s}$ shown in Figure 2(b). These two figures indicate that a larger extraction rate produces a lower aquifer temperature at the same radial distance.

Figure 3 shows the predicted curves of aquifer temperature (T_m) versus r at $t=10^3$, 5×10^3, 10^4, 2×10^4, 2×10^5 days, and at steady state for $(\rho c)_m=2.84\times10^6\,\mathrm{J/m^3\cdot K}$, $K_m=2.4\,\mathrm{W/m\cdot K}$, $b_m=10\,\mathrm{m}$, $T_b=23^\circ\mathrm{C}$, $T_{m0}=70^\circ\mathrm{C}$, and $Q=1\times10^{-4}\,\mathrm{m}^3/\mathrm{s}$. This figure shows that T_m decreases with increasing t and decreasing r. Under the same operating time, the aquifer temperature increases slightly near the extraction well, significantly at a radial distance ranging from 10 to 100 m, and then approaches a constant value at $r>100\,\mathrm{m}$. The results also show that the values of extracted temperature (T_w) are 69.4, 61.5, 50.2, 36.8, and 22.8°C at $t=10^3$, 5×10^3, 10^4, 2×10^4, and 2×10^5 days, respectively. In addition, the aquifer temperature maintains constant values in the regions after $r=30$, 80, 100, 130, and 200 m at $t=10^3$, 5×10^3, 10^4, 2×10^4, and 2×10^5 days, respectively. If one defines the heat extraction efficiency (η) as T_w/T_{m0}, then its values are 0.99, 0.88, 0.72, 0.53, and 0.33 at $t=10^3$, 5×10^3, 10^4, 2×10^4, and 2×10^5 days, respectively. This shows that η decreases with t. In addition, the aquifer temperature distribution over a long period of time (say $t=2\times10^5$ days) agrees with that of the steady-state solution. This indicates that there is no advective heat transfer in the ATE system when t is very large.

Figure 4 shows the predicted curves of extracted temperature (T_w) versus t for aquifer thickness $b_m=10$ and 30 m with various values of geothermal gradients g_1 and g_2. When $g_1=g_2=0^\circ\mathrm{C/m}$ (denoted by the solid line), a larger b_m yields a higher T_w from 10^3 to 2×10^5 days. In this period, T_w is significantly affected by the aquifer thickness due to the thermal capacity (i.e. the product of density and specific heat, ρc) per unit thickness. When $g_1=0.03^\circ\mathrm{C/m}$ and $g_2=0.06^\circ\mathrm{C/m}$ (denoted by the dashed line), the curves of T_w versus t are represented with a circle symbol for case 1 ($b_m=10\,\mathrm{m}$) and with a star symbol for case 2 ($b_m=30\,\mathrm{m}$). This figure shows that a smaller b_m yields a higher T_w when $t<10^3$ days, indicating that the heat transfer at the interface of the aquifer and rocks is quick for case 1. However, the difference of T_w between cases 1 and 2 is dependent on the geothermal gradient and thermal conductivity. On the other hand, a larger b_m yields a higher T_w when $t>10^3$ days, implying that a larger b_m yields a higher thermal capacity per unit thickness. Moreover, the figure also shows that T_w approaches 22.0°C for the case of $g_1=g_2=0^\circ\mathrm{C/m}$ and 22.8°C for the case of $g_1=0.03^\circ\mathrm{C/m}$ and $g_2=0.06^\circ\mathrm{C/m}$ when $t\geqslant2\times10^5$ days. Obviously, the geothermal gradient of the rocks has a significant effect on the extracted temperature.

The curves of T_w versus t for various values of b_m and the outer surface temperature of the overlying rock (T_{20}) are plotted in Figure 5. The figure shows that T_w increases with decreasing t. It also shows that T_w remains constant when $t\leqslant10^3$ days and a larger T_{20} yields a higher T_w when $t>10^3$ days for the same b_m. In addition, the difference of T_w between the cases of $b_m=10$ and 30 m increases with t when t ranges from 10^3 to 2×10^5 days and approaches a constant when $t\geqslant2\times10^5$ days. For a fixed value of T_{20}, the curve of T_w versus t is represented with a circle

DOI: 10.1002/nag

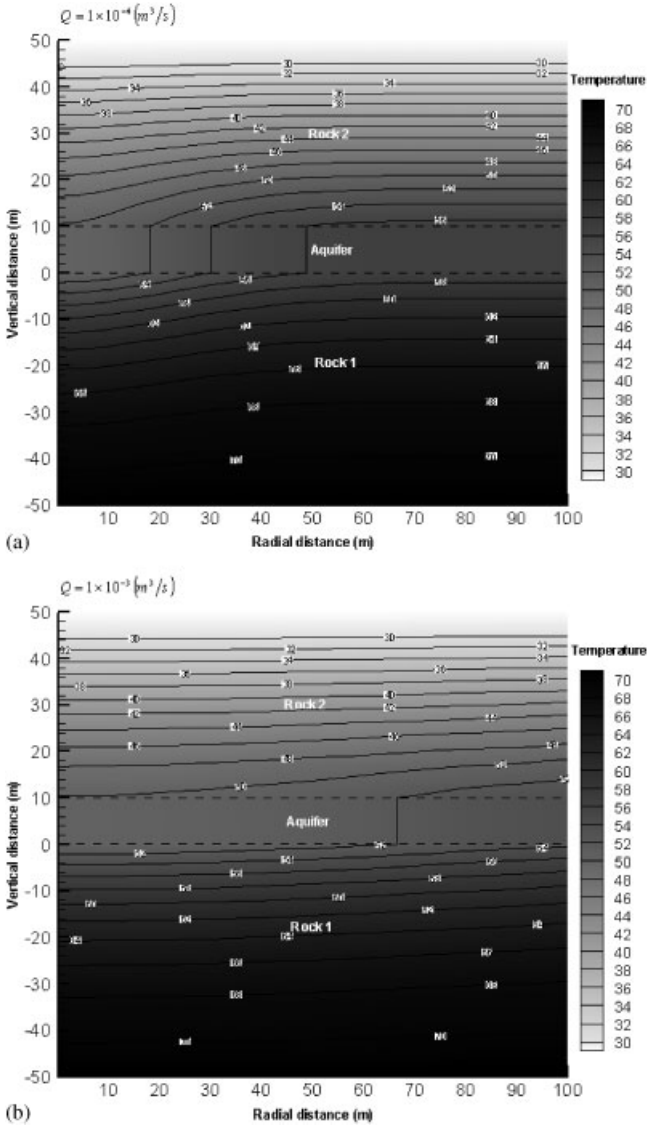

Figure 2. The temperature distribution in the ATE system at $t = 10^4$ days for $h_1 = 0.6\,\mathrm{W/m^2 \cdot K}$, $h_2 = 1.0\,\mathrm{W/m^2 \cdot K}$, and $Q =$ (a) $1 \times 10^{-4}\,\mathrm{m^3/s}$ and (b) $1 \times 10^{-3}\,\mathrm{m^3/s}$.

symbol for the $b_m = 10\,\mathrm{m}$ case and with a star symbol for the $b_m = 30\,\mathrm{m}$ case. The figure also shows that a smaller b_m yields a higher T_w when $t < 2 \times 10^3$ days for the $T_{20} = 50^\circ\mathrm{C}$ case and $t < 1 \times 10^3$ days for the $T_{20} = 30^\circ\mathrm{C}$ case. On the other hand, a larger b_m yields a higher T_w when $t > 2 \times 10^3$ days for the $T_{20} = 50^\circ\mathrm{C}$ case and $t > 1 \times 10^3$ days for the $T_{20} = 30^\circ\mathrm{C}$ case. Obviously, a thicker aquifer yields higher heat energy per unit thickness. It is evident that T_w approaches $50.3^\circ\mathrm{C}$ for the $T_{20} = 50^\circ\mathrm{C}$ case and $29.9^\circ\mathrm{C}$ for the $T_{20} = 30^\circ\mathrm{C}$ case when $t \geqslant 2 \times 10^5$ days. Finally, it can be concluded that the outer surface temperature has significant impact on aquifer temperature for t ranging from 10^3 to 2×10^5 days.

5. CONCLUSIONS

A mathematical model is developed to simulate the temperature distribution for extracting hot water from geothermal confined aquifers. Based on the model, a semi-analytical solution is developed to predict the dimensionless temperature distributions in the aquifer as well as the underlying and

DOI: 10.1002/nag

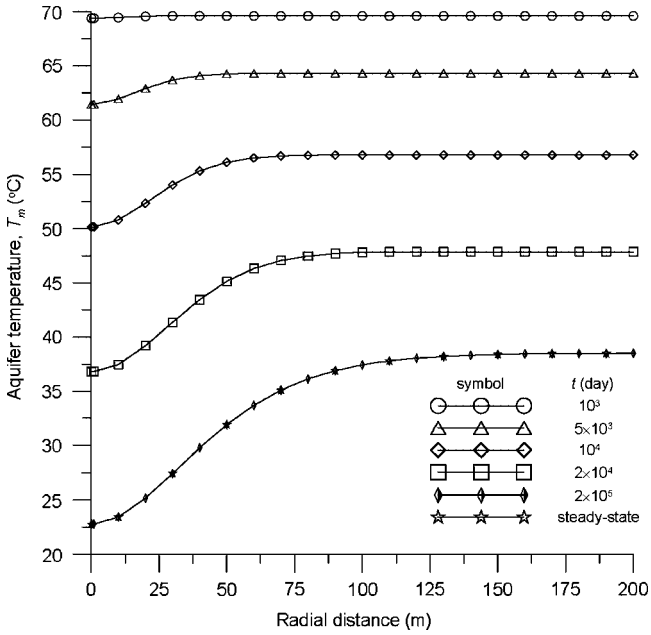

Figure 3. Curves of aquifer temperature (T_m) versus radial distance (r) predicted by the transient solution (Equation (13)) at $t = 10^3$, 5×10^3, 10^4, 2×10^4, and 2×10^5 days and by the steady-state solution (Equation (18)) for $(\rho c)_m = 2.84 \times 10^6 \, \mathrm{J/m^3 \cdot K}$, $K_m = 2.4 \, \mathrm{W/m \cdot K}$, $b_m = 10 \, \mathrm{m}$, $T_b = 23^\circ\mathrm{C}$, $T_{m0} = 70^\circ\mathrm{C}$, and $Q = 1 \times 10^{-4} \, \mathrm{m^3/s}$.

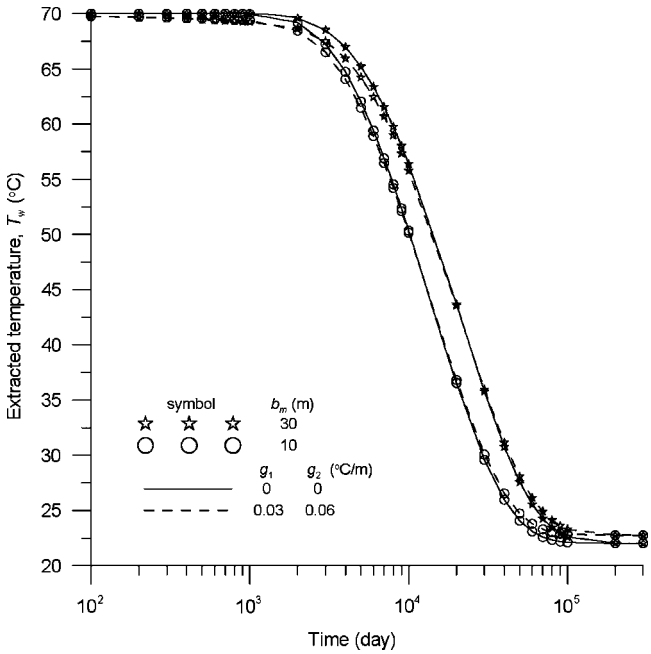

Figure 4. Curves of extracted temperature (T_w) versus operating time (t) for various values of aquifer thickness and geothermal gradient.

overlying rocks. The time-domain results are computed numerically by the modified Crump method with accuracy to the fourth decimal. In addition, the steady-state solution is also provided in this study. The analyzed results have revealed several important points. The extraction rate, aquifer

DOI: 10.1002/nag

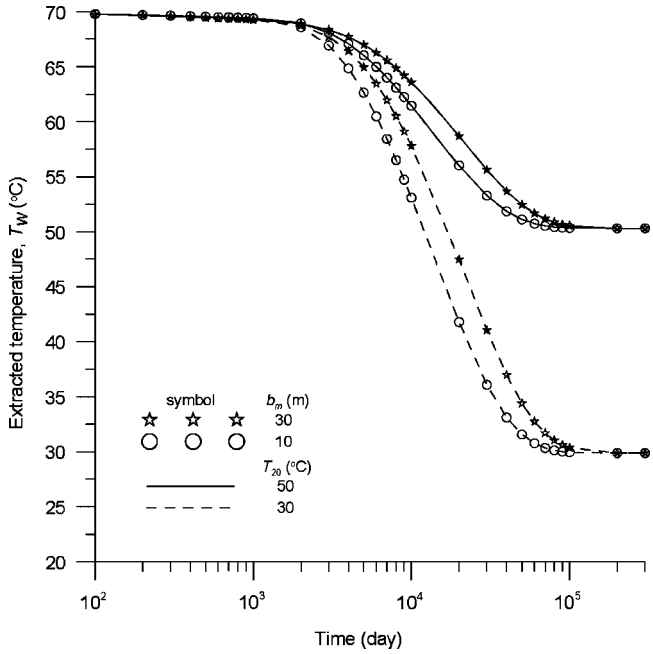

Figure 5. Curves of extracted temperature (T_w) versus operating time (t) for the cases of $T_{20}=30$ and 50°C when the aquifer thickness (b_m) is 10 or 30 m.

thickness, geothermal gradient, and outer temperature of the rocks have significant impacts on the extracted temperature in the ATE system. The transient solution matches with the steady-state solution when the operating time is longer than 2×10^5 days. In addition, the convective heat transfer coefficient affects the rock temperature distribution only near the outer boundaries of the rocks.

The solution can be used to assess the effects of extraction rate, thermomechanical properties, aquifer thickness, geothermal gradient, outer rock surface temperature, and convective heat transfer coefficient on the aquifer temperature distributions. The solution can also be applied to assess the spatial and temporal temperature distributions in the aquifer and adjacent rocks in ATE systems. Accordingly, this solution can be used for designing an efficient ATE system to extract geothermal energy for power generation or hot springs for tourism. Note that the effect of rock deformation on fluid flow and thermal convection, not included in our conceptual model, should be considered if the rock deformation produced by well discharge is large.

APPENDIX A: DEVELOPMENT OF THE SOLUTIONS (13), (16), AND (17)

Equations (1)–(12) can be expressed in dimensionless forms using dimensionless parameters given in Table I. The heat convection–conduction equation describing the aquifer temperature in dimensionless form can thus be expressed as

$$\frac{\partial^2 T_{mD}(R,\tau)}{\partial R^2}+\left(\frac{1-2v}{R}\right)\frac{\partial T_{mD}(R,\tau)}{\partial R}+K_{1D}\left.\frac{\partial T_{1D}(R,Z_1,\tau)}{\partial Z_1}\right|_{Z_1=0}+K_{2D}\left.\frac{\partial T_{2D}(R,Z_2,\tau)}{\partial Z_2}\right|_{Z_2=0}=\frac{\partial T_{mD}(R,\tau)}{\partial \tau} \tag{A1}$$

The dimensionless forms for the initial and boundary conditions are

$$T_{mD}(R,0)=0 \tag{A2}$$

$$\frac{\partial T_{mD}(R_w,\tau)}{\partial R}=\left(\frac{2v}{R_w}\right)T_{mD}(R_w,\tau) \tag{A3}$$

DOI: 10.1002/nag

and

$$T_{mD}(\infty,\tau)=0 \tag{A4}$$

The heat conduction equation describing the dimensionless temperature distribution in the underlying rock can be written as

$$\frac{\partial^2 T_{1D}(R,Z_1,\tau)}{\partial Z_1^2}=\frac{1}{\alpha_{1D}}\frac{\partial T_{1D}(R,Z_1,\tau)}{\partial \tau},\quad 0<Z_1<4B_1 \tag{A5}$$

where $\alpha_{1D}=4\alpha_1/\alpha_m$ and $Z_1=-4z/b_m$. The dimensionless initial and boundary conditions are

$$T_{1D}(R,Z_1,0)=T_{1g}Z_1 \tag{A6}$$

$$T_{1D}(R,0,\tau)=T_{mD}(R,\tau) \tag{A7}$$

and

$$\frac{\partial T_{1D}(R,4B_1,\tau)}{\partial Z_1}=-\frac{\beta_1}{4}[T_{1D}(R,4B_1,\tau)-T_{10D}] \tag{A8}$$

where $T_{10D}=(T_{10}-T_{m0})/(T_b-T_{m0})$, $B_1=b_1/b_m$, and $\beta_1=h_1 b_m/K_1$.

Similarly, the heat conduction equation describing the dimensionless temperature distribution in the overlying rock is

$$\frac{\partial^2 T_{2D}(R,Z_2,\tau)}{\partial Z_2^2}=\frac{1}{\alpha_{2D}}\frac{\partial T_{2D}(R,Z_2,\tau)}{\partial \tau},\quad 0<Z_2<4B_2 \tag{A9}$$

where $\alpha_{2D}=4\alpha_2/\alpha_m$ and $Z_2=4(z-b_m)/b_m$. The dimensionless initial and boundary conditions are

$$T_{2D}(R,Z_2,0)=-T_{2g}Z_2 \tag{A10}$$

$$T_{2D}(R,0,\tau)=T_{mD}(R,\tau) \tag{A11}$$

and

$$\frac{\partial T_{2D}(R,4B_2,\tau)}{\partial Z_2}=-\frac{\beta_2}{4}[T_{2D}(R,4B_2,\tau)-T_{20D}] \tag{A12}$$

where $T_{20D}=(T_{20}-T_{m0})/(T_b-T_{m0})$, $B_2=b_2/b_m$, and $\beta_2=h_2 b_m/K_2$.

Taking Laplace transforms of Equations (A1), (A3), and (A4), respectively, yield

$$\frac{\mathrm{d}^2\overline{T}_{mD}(R,p)}{\mathrm{d}R^2}+\left(\frac{1-2v}{R}\right)\frac{\mathrm{d}\overline{T}_{mD}(R,p)}{\mathrm{d}R}+K_{1D}\left.\frac{\mathrm{d}\overline{T}_{1D}(R,Z_1,p)}{\mathrm{d}Z_1}\right|_{Z_1=0}$$

$$+K_{2D}\left.\frac{\mathrm{d}\overline{T}_{2D}(R,Z_2,p)}{\mathrm{d}Z_2}\right|_{Z_2=0}=p\overline{T}_{mD}(R,p) \tag{A13}$$

$$\frac{\mathrm{d}\bar{T}_{mD}(R_\mathrm{w},p)}{\mathrm{d}R}=\left(\frac{2v}{R_\mathrm{w}}\right)\bar{T}_{mD}(R_\mathrm{w},p) \tag{A14}$$

and

$$\bar{T}_{mD}(\infty,p)=0 \tag{A15}$$

Moreover, taking Laplace transforms of Equations (A5), (A7), and (A8), respectively, lead to

$$\frac{\mathrm{d}^2\bar{T}_{1D}(R,Z_1,p)}{\mathrm{d}Z_1^2}=q_1^2\bar{T}_{1D}(R,Z_1,p)-\gamma_1^2 Z_1 \tag{A16}$$

$$\bar{T}_{1D}(R,0,p)=\bar{T}_{mD}(R,p) \tag{A17}$$

DOI: 10.1002/nag

and

$$\frac{\mathrm{d}\bar{T}_{1D}(R,4B_1,p)}{\mathrm{d}Z_1}=-\frac{\beta_1}{4}\bar{T}_{1D}(R,4B_1,p)+\frac{\beta_1}{4p}T_{10D} \tag{A18}$$

where $q_1^2=p/\alpha_{1D}$ and $\gamma_1^2=T_{1g}/\alpha_{1D}$.

Similarly, taking Laplace transforms of Equations (A9), (A11), and (A12), respectively, obtains

$$\frac{\mathrm{d}^2\bar{T}_{2D}(R,Z_2,p)}{\mathrm{d}Z_2^2}=q_2^2\bar{T}_{2D}(R,Z_2,p)+\gamma_2^2Z_2 \tag{A19}$$

$$\bar{T}_{2D}(R,0,p)=\bar{T}_{mD}(R,p) \tag{A20}$$

and

$$\frac{\mathrm{d}\bar{T}_{2D}(R,4B_2,p)}{\mathrm{d}Z_2}=-\frac{\beta_2}{4}\bar{T}_{2D}(R,4B_2,p)+\frac{\beta_2}{4p}T_{20D} \tag{A21}$$

where $q_2^2=p/\alpha_{2D}$ and $\gamma_2^2=T_{2g}/\alpha_{2D}$.

Equations (A16) and (A19) are linear differential equations and thus can be solved by the superposition principle. Their solutions in the Laplace domain consist of the homogeneous solution, $\overline{T}^h_{1D}$, and the nonhomogeneous solution, $\overline{T}^p_{1D}$. That is

$$\overline{T}_{1D}=\overline{T}^h_{1D}+\overline{T}^p_{1D} \tag{A22}$$

The Laplace-domain solution of Equation (A16) for temperature distribution in the underlying rock is

$$\overline{T}_{1D}=C_1\cosh q_1Z_1+C_2\sinh q_1Z_1+\frac{T_{1g}}{p}Z_1 \tag{A23}$$

where C_1 and C_2 are the undetermined constants. Substituting Equation (A23) into Equations (A17) and (A18) and taking some algebraic manipulations, the undetermined constants can then be determined as

$$C_1=\bar{T}_{mD}(R,p) \tag{A24}$$

and

$$C_2=-\bar{T}_{mD}(R,p)x_1-\frac{y_1}{p}[4T_{1g}(1+\beta_1B_1)-\beta_1T_{10D}] \tag{A25}$$

where $x_1=[4q_1\sinh(4q_1B_1)+\beta_1\cosh(4q_1B_1)]y_1$ and $y_1=1/[4q_1\cosh(4q_1B_1)+\beta_1\sinh(4q_1B_1)]$. Equation (16) can be obtained by substituting the constants of Equations (24) and (25) into Equation (23). Similarly, the Laplace-domain solution for the overlying rock, Equation (17), can be obtained from Equations (A19)–(A21).

Substituting Equations (16) and (17) into Equation (A13), one obtains

$$\frac{\mathrm{d}^2\overline{T}_{mD}(R,p)}{\mathrm{d}R^2}+\left(\frac{1-2v}{R}\right)\frac{\mathrm{d}\overline{T}_{mD}(R,p)}{\mathrm{d}R}-A(p)\overline{T}_{mD}(R,p)=\frac{1}{p}B(p) \tag{A26}$$

where the functions of $A(p)$ and $B(p)$ in Equation (A26) are given as Equations (14) and (15), respectively. Equation (A26) is a linear differential equation which can also be solved by applying the superposition principle. The Laplace-domain solution of Equation (A26) consisting of the homogeneous solution, $\overline{T}^h_{mD}$, and nonhomogeneous solution, $\overline{T}^p_{mD}$, can be expressed as

$$\overline{T}_{mD}=\overline{T}^h_{mD}+\overline{T}^p_{mD} \tag{A27}$$

DOI: 10.1002/nag

The homogeneous equation in Equation (A27) is a special form of Bessel equation and its general solution is

$$\overline{T}^{h}_{mD} = R^{-v}[D_1 I_v(\sqrt{A(p)}R) + D_2 K_v(\sqrt{A(p)}R)] \tag{A28}$$

where v is equal to $-Q(\rho c)_m/(4\pi n b_m K_m)$; D_1 and D_2 are the undetermined constants; $I_v(\cdot)$ and $K_v(\cdot)$ are the modified Bessel function of the first and second kinds with order v, respectively. The nonhomogeneous equation in Equation (A27) can be easily solved and its particular solution is

$$\overline{T}^{p}_{mD} = -\frac{B(p)}{pA(p)} \tag{A29}$$

Based on the superposition principle, the Laplace-domain solution can then be obtained from substituting Equations (A28) and (A28) into Equation (A27) as

$$\overline{T}_{mD} = R^{-v}[D_1 I_v(\sqrt{A(p)}R) + D_2 K_v(\sqrt{A(p)}R)] - \frac{B(p)}{pA(p)} \tag{A30}$$

Substituting Equation (A30) into Equations (A14) and (A15), the constants of D_1 and D_2 can be determined as

$$D_1 = 0 \tag{A31}$$

and

$$D_2 = -\frac{R_w^v}{p}\left[\frac{2v}{2vK_v(\sqrt{A(p)}R_w) + (\sqrt{A(p)}R_w)K_{v-1}(\sqrt{A(p)}R_w)}\right]\left[\frac{B(p)}{A(p)}\right] \tag{A32}$$

The dimensionless aquifer temperature distribution in Equation (13) can then be obtained from substituting Equations (A31) and (A32) into Equation (A30).

APPENDIX B: DEVELOPMENT OF EQUATION (18)

The steady-state solution can be obtained from the transient solution when applying the final value theorem [16] as

$$T_{mD}(R,\infty) = \lim_{p\to 0} p\bar{T}_{mD}(R,p) \tag{B1}$$

Accordingly, substituting Equation (13) into Equation (B1) yields

$$T_{mD}(R,\infty) = \lim_{p\to 0}\left\{-\left(\frac{R_w}{R}\right)^v\left[\frac{2vK_v(\sqrt{A(p)}R)}{2vK_v(\sqrt{A(p)}R_w) + (\sqrt{A(p)}R_w)K_{v-1}(\sqrt{A(p)}R_w)}\right]\left[\frac{B(p)}{A(p)}\right] - \frac{B(p)}{A(p)}\right\} \tag{B2}$$

The hyperbolic functions given by Abramowitz and Stegun [21, p. 85] are

$$\sinh(\zeta) = \zeta + \frac{\zeta^3}{3!} + \frac{\zeta^5}{5!} + \frac{\zeta^7}{7!} + \cdots \quad (|\zeta| < \infty) \tag{B3}$$

and

$$\cosh(\zeta) = 1 + \frac{\zeta^2}{2!} + \frac{\zeta^4}{4!} + \frac{\zeta^6}{6!} + \cdots \quad (|\zeta| < \infty) \tag{B4}$$

Set $\zeta_1 = (4q_1 B_1)$ and $\zeta_2 = (4q_2 B_2)$ and let $p \to 0$ for Equations (B3) and (B4). Then, Equations (14) and (15) reduce to Equations (19) and (20), respectively. Substituting Equations (19) and (20) into Equation (B2) leads to the steady-state solution of dimensionless aquifer temperature presented in the text as Equation (18).

DOI: 10.1002/nag

NOTATION

b_i	thickness, m, $i=1$, 2, or m
B_i	b_i/b_m, $i=1$, 2; dimensionless thickness
g_i	geothermal gradient, °C/m, $i=1$, 2
h_i	convective heat transfer coefficient, W/m^2·K, $i=1$, 2
K_i	thermal conductivity, W/m·K, $i=1$, 2, or m
K_{iD}	K_i/K_m, $i=1$, 2; dimensionless thermal conductivity
p	Laplace transform variable
q_i^2	p/α_{iD}, $i=1$, 2
Q	extraction rate, m^3/s
r	radial distance from the center of extraction well, m
r_w	wellbore radius, m
R	$2r/b_m$; dimensionless radial distance from the center of extraction well
R_w	$2r_w/b_m$; dimensionless wellbore radius
t	operating time, s
T_i	temperature, °C, $i=1$, 2, m, or b
T_{iD}	$(T_i-T_{m0})/(T_b-T_{m0})$, i = 1, 2, or m; dimensionless temperature
T_{ig}	$g_i b_m/4(T_b-T_{m0})$, $i=1$, 2; dimensionless geothermal gradient
$\bar{T}_{iD}$	dimensionless temperature in Laplace domain, i = 1, 2, or m
u	$-Q/(2\pi r n b_m)$; volumetric flux per unit pore area, m/s
v	$-Q(\rho c)_m/(4\pi n b_m K_m)$; dimensionless convective parameter
z	vertical distance from the bottom of the aquifer, m
Z_1	$-4z/b_m$; dimensionless vertical distance from the bottom of the aquifer to the underlying rock
Z_2	$4(z-b_m)/b_m$; dimensionless vertical distance from the bottom of the aquifer to the overlying rock
α_i	$K_i/(\rho c)_i$, $i=1$, 2, or m; thermal diffusivity, m^2/s
α_{iD}	$4\alpha_i/\alpha_m$, $i=1$, 2; dimensionless thermal diffusivity
β_i	$h_i b_m/K_i$, i = 1, 2; Biot number
γ_i^2	T_{ig}/α_{iD}, $i=1$, 2
$(\rho c)_i$	thermal capacity, J/m^3·K, $i=1$, 2, or m
τ	$4\alpha_m t/b_m^2$; dimensionless operating time

Subscripts

b	atmospheric temperature of ground surface
m	aquifer
0	reference value
1	underlying rock
2	overlying rock

ACKNOWLEDGEMENTS

This study was supported by the Taiwan National Science Council under the contract numbers NSC 99-NU-E-009-001, NSC 99-2221-E-009-062-MY3, and NSC 99-2116-M-238-001.

REFERENCES

1. Sauty JP, Gringarten AC, Menjoz A, Landel PA. Sensible energy storage in aquifers 1. Theoretical study. *Water Resources Research* 1982; **18**(2):245–252.
2. Sauty JP, Gringarten AC, Fabris H, Thiery D, Menjoz A, Landel PA. Sensible energy storage in aquifers 2. Field experiments and comparison with theoretical results. *Water Resources Research* 1982; **18**(2):253–265.
3. Carotenuto A, Casarosa C, Martorano L. The geothermal convector: experimental and numerical results. *Applied Thermal Engineering* 1999; **19**:349–374.

DOI: 10.1002/nag

4. Tenma N, Yasukawa K, Zyvoloski G. Model study of the thermal storage system by FEHM. *Geothermics* 2003; **32**:603–607.
5. Zyvoloski GA, Robinson BA, Dash ZV, Trease LL. User's Manual for the FEHM Application—A Finite-Element Heat- and Mass-Transfer Code (LA-13306-M). Los Alamos National Laboratory, NM, 1997.
6. Tenma N, Yamaguchi T, Zyvoloski G. The Hijiori Hot Dry Rock test site, Japan Evaluation and optimization of heat extraction from a two-layered reservoir. *Geothermics* 2008; **37**:19–52.
7. Yang SY, Yeh HD. An analytical solution for modeling thermal energy transfer in a confined aquifer system. *Hydrogeology Journal* 2008; **16**:1507–1515.
8. Yang SY, Yeh HD. Modeling heat extraction from hot dry rock in a multi-well system. *Applied Thermal Engineering* 2009; **29**:1676–1681.
9. Ghassemi A, Tarasovs A, Cheng AH-D. An integral equation solution for three-dimensional heat extraction from planar fracture in hot dry rock. *International Journal for Numerical and Analytical Methods in Geomechanics* 2003; **27**:989–1004.
10. Ghassemi A, Kumar GS. Changes in fracture aperture and fluid pressure due to thermal stress and silica dissolution/precipitation induced by heat extraction from subsurface rocks. *Geothermics* 2007; **36**:115–140.
11. Ghassemi A, Nygren A, Cheng AH-D. Effects of heat extraction on fracture aperture: a poro-thermoelastic analysis. *Geothermics* 2008; **37**:525–539.
12. Yin S, Dusseault MB, Rothenburg L. Thermal reservoir modeling in petroleum geomechanics. *International Journal for Numerical and Analytical Methods in Geomechanics* 2009; **33**:449–485.
13. Crump KS. Numerical inversion of Laplace transforms using a Fourier series approximation. *Journal of the ACM* 1976; **23**(1):89–96.
14. de Hoog FR, Knight JH, Stokes AN. An improved method for numerical inversion of Laplace transforms. *SIAM Journal on Scientific and Statistical Computing* 1982; **3**(3):357–366.
15. Özisik MN. *Heat Conduction* (2nd edn). Wiley: New York, 1993.
16. Carslaw HS, Jaeger JC. *Conduction of Heat in Solids* (2nd edn). Oxford University Press: London, 1959.
17. Arpaci VS. *Conduction Heat Transfer*. Addison & Wesley Inc: Reading, MA, 1966.
18. Spiegel MR. *Schaum's outline of Theory and Problems of Laplace Transforms*. Schaum: New York, 1965.
19. Yeh HD, Wang CT. Large-time solutions for groundwater flow problems using the relationship of small p versus large t. *Water Resources Research* 2007; **43**(6):W06502, 1–6.
20. IMSL. IMSL Fortran Library User's Guide Math/Library Volume 2 of 2, version 5.0. Visual Numerics: Houston, TX, 2003.
21. Chen JS, Liu CW, Chen CS, Yeh HD. A Laplace transform solution for tracer tests in a radially convergent flow field with upstream dispersion. *Journal of Hydrology* 1996; **183**:263–275.
22. Yeh HD, Yang SY. A novel analytical solution for a slug test conducted in a well with a finite-thickness skin. *Advances in Water Resources* 2006; **29**(10):1479–1489.
23. Shanks D. Non-linear transformations of divergent and slowly convergent sequences. *Journal of Mathematical Physics* 1955; **34**:1–42.
24. Abramowitz M, Stegun IA. *Handbook of Mathematical Functions with Formulas, Graphs and Mathematical Tables*. National Bureau of Standards: Dover, WA, 1964.
25. Yang SY, Yeh HD. A closed-form solution for a confined flow into a tunnel during progressive drilling in a multi-layer groundwater flow system. *Geophysical Research Letters* 2007; **34**(7):L07405, 1–5.
26. Yeh HD, Chang YC, Zlotnik VA. Stream depletion rate and volume from groundwater pumping in wedge-shape aquifers. *Journal of Hydrology* 2008; **349**(3–4):501–511.

DOI: 10.1002/nag